Modified Voronoi Analysis of Spontaneous Formation of Interfacial Droplets on Immersed Oil-Solid Substrates

Zhang, Ran; Mei, Ran Andy; Botto, Lorenzo; Yang, Zhongqiang

DOI
10.1021/acs.langmuir.9b03806

Publication date
2020

Document Version
Final published version

Published in
Langmuir : the ACS journal of surfaces and colloids

LANGMUIR

pubs.acs.org/Langmuir Article

Modified Voronoi Analysis of Spontaneous Formation of Interfacial Droplets on Immersed Oil–Solid Substrates

Ran Zhang, Ran Andy Mei, Lorenzo Botto, and Zhongqiang Yang*

Cite This: *Langmuir* 2020, 36, 5400–5407 Read Online

ACCESS | Metrics & More | Article Recommendations | Supporting Information

ABSTRACT: The nucleation and growth of liquid droplets on solid substrates have received much attention because of the significant relevance of these multiphase processes to both nature and practical applications. There have been extensive studies on the condensation of water from the air phase on solid substrates. Here, we focus on water diffusion through the oil phase and subsequent settlement on solid substrates because such interfacial droplets are formed. Voronoi diagram analysis is proposed to statistically characterize the size distribution of the growing droplets. It is found that modification of the standard Voronoi diagram is required for systems of interfacial droplets which have a noncircular shape and/or whose centers change with time. The modified Voronoi analysis of the growing droplets provides an automatic quantification of the droplet distribution and reveals that (i) during the nucleation stage, the interfacial droplets do not nucleate at the same time because the nucleation of newly formed droplets competes with the growth of the existing ones; (ii) the growth of interfacial droplets comes from water diffusion from the bulk water layer, and/or from adjacent interfacial droplets, and/or from coalescence of interfacial droplets; and (iii) the sizes of interfacial droplets become more polydispersed on P-glass but more monodispersed on OTS-glass as time goes. This work opens a new perspective on the formation of interfacial droplets at the interface between oil and the solid substrate and demonstrates the capability of an automatic analysis method, which can be potentially applied to similar interfacial multiphase systems.

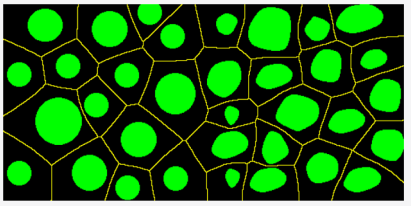

INTRODUCTION

There is growing interest in the controlled formation of droplets on solid substrates,[1−8] for applications such as the fabrication of microstructured surfaces,[9,10] controlled condensation,[11,12] cooling,[13,14] and fog harvesting.[15−18] Studies on a single droplet or a few droplets have enabled advancements in our understanding of processes such as contact line pinning,[19,20] droplet growth,[21−23] and coalescence.[24−27] However, the droplet behavior in realistic systems is controlled by complex many-body interactions, and is extremely sensitive to initial conditions,[28−31] making a statistical analysis via automatic techniques necessary. A valuable technique for the automatic image analysis of a large number of droplets on solid substrates is the Voronoi diagram analysis, used by Zhang, Lohse, and collaborators, for example, to study the size and the spatial distribution of surface nanobubbles and nanodroplets.[21,32,33] In their experiments, nanobubbles and nanodroplets were produced by a solvent exchange process, and Voronoi diagram analysis helped them gather information on the mechanism and formation of nanobubbles and nanodroplets. In this paper, we focus on the analysis of interfacial droplets grown spontaneously at an oil–solid interface by water diffusion through an oil layer.[26,34,35] In a typical experiment, an *n*-hexadecane layer of several tens of micrometer thickness is deposited onto a hydrophilic or hydrophobic substrate and then submerged in water. Just after a few minutes, water diffuses through the oil layer and condenses on the hydrophilic or hydrophobic glass in the form of tiny interfacial droplets. The aim of this current paper is to apply Voronoi analysis to our experimental system, to characterize the mechanisms leading to nucleation and growth in such a system, and to illustrate the strengths of the Voronoi approach. The proposed analysis will not only be valuable for others to characterize similar systems but also provide important insights into our particular multiphase system, a configuration for which very little information is available in the literature.

EXPERIMENTAL SECTION

Materials. The glass coverslips (22 × 22 mm, Cat., #72204-1) and gold grids (20 μm thickness, 333 μm pitch, and 55 μm bar width) were obtained from Electron Microscopy Sciences (Hatfield, PA, USA). *n*-Hexadecane (99%) was purchased from Alfa Aesar (Ward Hill, MA, USA). Octadecyltrichlorosilane (OTS) and calcein AM were purchased from Sigma-Aldrich (Milwaukee, WI, USA). Heptane (high-performance liquid chromatography grade) was purchased from Fisher Scientific (Pittsburgh, PA, USA). Culture dishes (35 × 12 mm, Nest, Cat., #706001) were purchased from Nest (Jiangsu, China). Other chemicals were obtained from local companies with A.R. grade or above. Milli-Q water (18.2 MΩ·cm) was used.

Received: December 10, 2019
Revised: April 25, 2020
Published: April 26, 2020

https://dx.doi.org/10.1021/acs.langmuir.9b03806
Langmuir 2020, 36, 5400–5407

Modification of Substrates. The glass microscope coverslips were immersed in piranha solution, a mixture of H_2SO_4 and H_2O_2 (v/v = 7:3), and heated to 80 °C for an hour. Then, the coverslips were cooled to room temperature, rinsed with water, and then dried at 100 °C in an oven for an hour, resulting in piranha-cleaned glass (P-glass). The P-glass was put in a 5 mM OTS heptane solution for 30 min, then rinsed in heptane, and dried at 100 °C in an oven for an hour. As a result, OTS-treated glass (OTS-glass) was obtained.

Formation of Interfacial Droplets. The protocol shown in Figure 1 was adopted from a previous publication.[26] First, the substrates were stuck onto the bottom of culture dishes containing a 10 mm diameter hole. Second, gold grids were put on modified solid substrates. Third, *n*-hexadecane was dripped onto grids, and the excess was removed using a 10 μL syringe in order to obtain a uniformly filled grid. We chose *n*-hexadecane as the oil phase because it is a pure single component, with a stated and monodispersed molecular weight. Finally, 4 mL of Milli-Q water was gently poured into culture dishes. The sample was incubated in an environmental chamber (temperature: 25 °C; relative humidity: 50%).

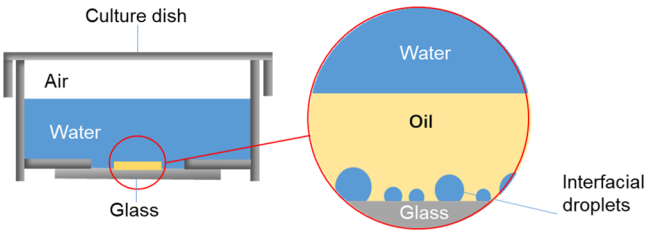

Figure 1. Schematic illustration of the experimental setup for the formation of interfacial droplets.

Optical and Confocal Imaging of Interfacial Droplets. In order to obtain fluorescent images of interfacial droplets, the fluorescent dye, calcein AM, was added into the upper aqueous solution to get a final concentration of 2 μM. The diffusion of the fluorescent dye into interfacial droplets enabled the visualization of interfacial droplets by inverted laser scanning confocal microscopy (LSCM) performed on a Zeiss LSM 800, model Airyscan (ex: 488 nm, em: 515 nm). The two-dimensional (2D) and three-dimensional (3D) confocal images were analyzed using ZEN blue software.

Standard Voronoi Diagram. The standard Voronoi diagram is based on the distance of the droplets' centers. The first step was to identify the droplets by applying a circle detection algorithm based on an in-built MATLAB command "imfindcircles". Through inputting the raw image, this function can output the position and the edge of circles in the original image. As a result, circular shapes of interfacial droplets were identified and drawn in red color on the image. Then, the center of the droplets could be determined, drawn as a black spot in the image. Using the circle data, "Voronoi" could be applied simply based on the center-point locations of the circles. The sides of each Voronoi cell shown in blue color were constructed from the perpendicular bisector to each center-to-center line. The MATLAB code is given in Supporting Information.

Modified Voronoi Diagram. The modified Voronoi diagram is constructed based on triple lines of droplets. In detail, the interfacial droplet shapes having significant color contrast with respect to the background were first identified using an in-built MATLAB command "im2bw", which can convert a grayscale image to a binary image. The conversion was to make the edge of interfacial droplets clearer, and the droplet shapes that were identified by software matched to the droplets in the image became far more accurate. Next, the modified Voronoi diagram drawn in yellow color was constructed based on the points equidistant to the two closest triple lines of droplets. The MATLAB code is shown in Supporting Information.

RESULTS AND DISCUSSION

Growth Behaviors. Interfacial droplets formed at the oil−solid interface, owing to the diffusion of water molecules through the micrometer thick oil layer and subsequent accumulation at the solid surface. The diffusion mechanism is illustrated in Figure 2. Initially, the water concentration at the oil−solid interface is negligible, while the concentration at the water−oil interface is at saturation, $c = c_s$. Under these conditions, the vertical mass flux from the water layer is maximum. As the droplets grow, the area-averaged concentration on the solid substrate increases ($c = c^* > 0$), hence the vertical diffusive flux decreases. As time proceeds, this increase in the water concentration at the solid substrate causes the system to approach saturation (a steady-state condition where all mass fluxes are zero). The difficulty in predicting the system's behavior is that, during growth, mass transfer also occurs laterally (red arrows in Figure 2). This lateral transport is due to the mass diffusion between noncontacting droplets and to droplet−droplet coalescence. Because of experimental limitations around micron resolution in an optical microscope, we could observe visible droplets only after roughly 2 min (see Figure S1), but it is likely that the initial formation of the droplets occurs much earlier. At the initial time, when the water concentration at the solid substrate is practically negligible, a diffusive mass flux drives water molecules at the rate $D\frac{dc}{dz} \cong D\frac{c_s}{h}$, where c_s is the saturation concentration of water in *n*-hexadecane, h is the *n*-hexadecane film thickness, and D is the diffusivity of water in *n*-hexadecane. As time progresses, the diffusive flux diminishes as the droplets grow in size and the average water concentration at the oil−solid interface increases. A rough estimate of the time scale t_d, characterizing the appearance of visible droplets, can be obtained from a simple mass balance by calculating the time. It would take a homogeneous water layer a thickness of a fraction of a visible droplet size (~1 μm) to form on the solid substrate. Calling h_d the thickness of such a homogeneous water layer and ρ_w the density of water, we obtain $t_d \approx \frac{h_d \rho_w h}{D c_s}$. The diffusion coefficient D of water in *n*-hexadecane is about 1.22×10^{-5} cm^2/s and the saturation concentration is about 564 g/m^3 at 25 °C.[36,37] From these data, we get, $t_d \approx 10$ s.

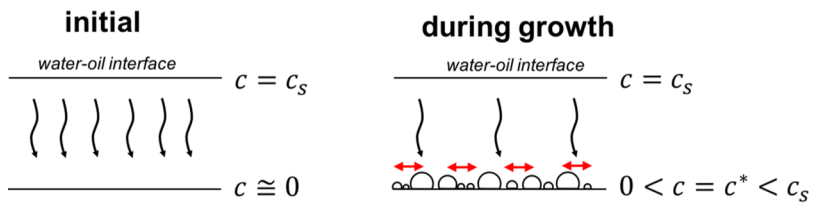

Figure 2. Diffusive mechanism of interfacial droplet growth. The mass flux driving the growth comes from the concentration difference between the water−oil interface and the solid substrate. The growth is modulated by the lateral diffusive flux between the droplets and the droplet−droplet coalescence.

https://dx.doi.org/10.1021/acs.langmuir.9b03806
Langmuir 2020, 36, 5400−5407

We explored the growth behaviors of interfacial droplets, focusing especially on the changes in the morphology and size of the droplets formed on solid substrates with different wettabilities. P-glass produced a hydrophilic surface, while OTS treatment turned the hydrophilic surface into a hydrophobic one and OTS-glass was obtained. In order to monitor the interfacial droplet growth *in situ*, LSCM was used. Figure 3 illustrates that interfacial droplets grown on P-glass for

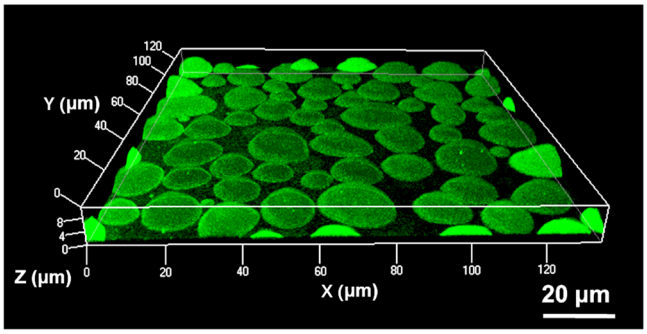

Figure 3. 3D image of interfacial droplets grown on P-glass when incubated in water for 8 days.

8 days appeared to be either ellipsoidal or irregular island-like, which can be attributed to the fast partial coalescence followed by a slow relaxation process. The strong contact-line pinning distorted the droplets to be irregular.[38] This observation was consistent with previous reports.[26,33] 3D images also reveal that the contact angle of interfacial droplets in *n*-hexadecane was about 40°, which was higher than that measured in air (<5°) because of the higher oil−solid surface tension than the air−solid surface tension. The growth process of interfacial droplets on P-glass is shown in Figure 4. To characterize the deviation from a spherical shape, we measured the maximal and minimal axes of interfacial droplets in 2D images, followed by calculating the corresponding aspect ratio (defined as the ratio of maximal to minimal axes). On day 8, the major axis was in the range 6−24 μm, while the aspect ratio varied from 1.0 to 2.0. Interfacial droplets absorbed water from the upper water layer or neighboring interfacial droplets, resulting in size increase. Besides, some droplets merged together and coalesced into bigger droplets. By day 12, the major axis increased to 10−32 μm. The maximum aspect ratio decreased from 2.0 to 1.6, suggesting that the shape of the droplets became less irregular. The interfacial droplets kept growing until day 16. The major axis on day 16 was in the range of 10−40 μm, and the maximum value of the aspect ratio further decreased to 1.4. After day 16, the interfacial droplets stopped growing.

Next, we examined the morphology of interfacial droplets grown on OTS-glass. It was observed that the interfacial droplets were spherical with the average aspect ratio remaining at 1.0 all the time. 3D images in Figure 5 show that the contact

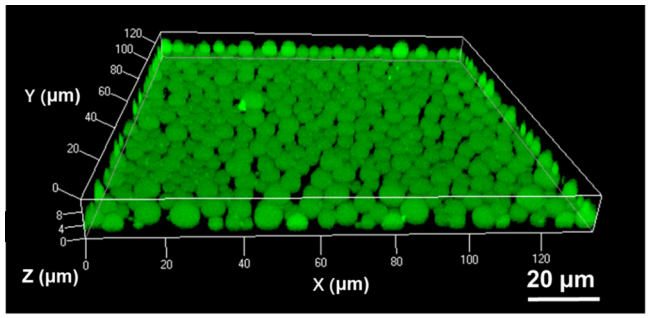

Figure 5. 3D image of interfacial droplets on OTS-glass when incubated in water for 8 days.

angle of interfacial droplets incubated for 8 days was nearly 130°, which was much higher than that on P-glass. This is because on OTS-glass, dewetting of water caused an interfacial droplet to assume a spherical shape; by comparison, the hydrophilicity of P-glass caused the interfacial droplets to spread much more. Figure 6 shows that the average diameter of interfacial droplets on OTS-glass was 3.3, 6.6, and 8.8 μm on days 8, 12, and 16, respectively. The interfacial droplets stopped growing after 16 days on OTS-glass. In summary, interfacial droplets can grow on both hydrophilic and hydrophobic substrates, and this further confirms the universality of substrates for this interfacial phenomenon. The morphology and size changes of interfacial droplets strongly rely on the wettability of the underlying solid substrates. Over a specific incubation period, the more hydrophilic the surface is, the more irregular and larger the interfacial droplets.

Standard Voronoi Diagram Analysis. In order to gain a more in-depth understanding of the interfacial phenomenon, we apply the Voronoi diagram analysis to characterize the spatial organization and growth behaviors of interfacial droplets on both P-glass and OTS-glass. The standard Voronoi diagram is drawn by MATLAB based on the distance of droplets' centers, and the detailed procedure is shown in the Experimental Section. In Figure 7, **a** refers to the projected area of the circles drawn in red. The area of the Voronoi cell comprising blue contours is denoted $\mathbf{A}_{\mathbf{vor}}$. However, on one side, owing to the hydrophilicity of the P-glass substrate, interfacial droplets appeared to be highly nonspherical. Hence, the contour detection step of the standard Voronoi analysis failed to precisely fit the projected shape of the droplets on this

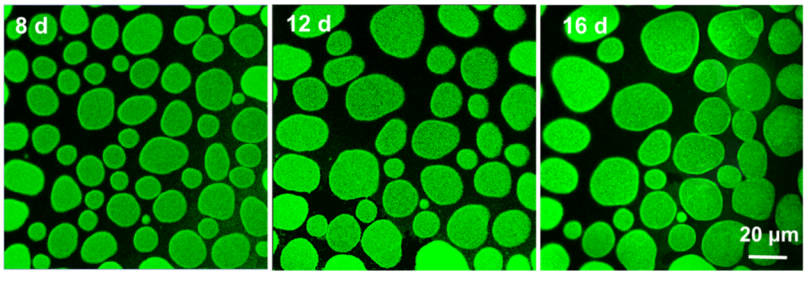

Figure 4. Fluorescent images of interfacial droplets grown on P-glass on days 8, 12, and 16.

https://dx.doi.org/10.1021/acs.langmuir.9b03806
Langmuir 2020, 36, 5400−5407

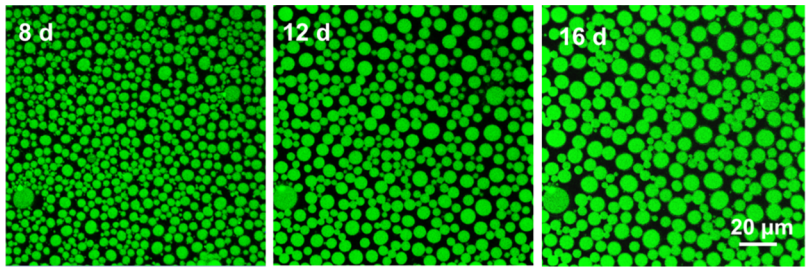

Figure 6. Fluorescent images of interfacial droplets grown on OTS-glass on days 8, 12, and 16.

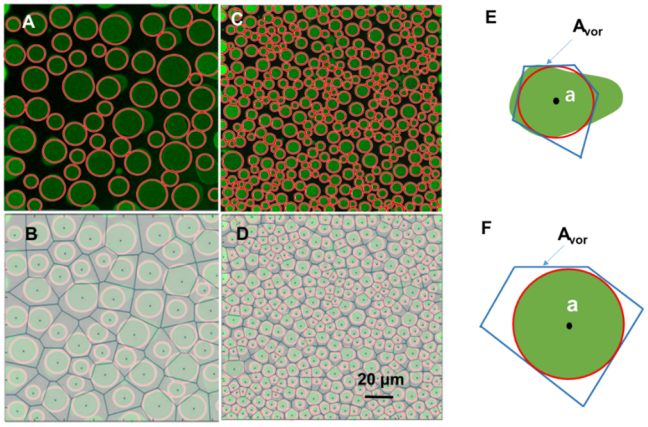

Figure 7. (A) Fluorescent images and (B) Voronoi diagram of interfacial droplets grown on P-glass on day 8. (C) Fluorescent images and (D) Voronoi diagram of interfacial droplets grown on OTS-glass on day 8. An example of **a** and $\mathbf{A}_{vor}$ of interfacial droplets formed on (E) P-glass and (F) OTS-glass; **a** is the projected area of the circle and $\mathbf{A}_{vor}$ is the area of the polygonal Voronoi cell.

substrate, as illustrated in Figure 7E. On the other side, in the standard Voronoi diagram, the cell area $\mathbf{A}_{vor}$ depends only on the droplets' centers. From Figure 6, we can find that on incubation, some interfacial droplets on OTS-glass only grew bigger in size, but did not change in the center. Hence, the standard Voronoi diagram could not detect the change in $\mathbf{A}_{vor}$ for interfacial droplets whose centers did not change with time. As a consequence, the standard Voronoi diagram is not suitable for analysis of the size of interfacial droplets based on a correlation between **a** and $\mathbf{A}_{vor}$ on both P-glass and OTS-glass. To overcome this limitation, we have adopted a modified Voronoi diagram approach.

Modified Voronoi Diagram Analysis. The modified Voronoi diagram is constructed based on the triple lines of interfacial droplets detected by the MATLAB algorithm. The detailed procedure is shown in Experimental Section. This feature is useful to characterize droplets with a nonspherical shape or droplets whose centers do not change with time. In a modified Voronoi diagram, **a** refers to the projected area of the circle drawn in green, while $\mathbf{A}_{vor}$ refers to the area of the polygonal Voronoi cell drawn in yellow. Modified Voronoi diagrams corresponding to days 8, 12, and 16 for interfacial droplets grown on P-glass are shown in Figure 8. It demonstrates that each interfacial droplet is associated with a single modified Voronoi cell.

Using image analysis, we computed **a** and $\mathbf{A}_{vor}$ for interfacial droplets grown on P-glass and analyzed their statistical relations via a scatter plot, as shown in Figure 9. The plot includes droplets in a given area of 135 μm × 135 μm. Each symbol in the plot corresponds to one droplet. Browsing from the top to the bottom in Figure 9, it can be clearly seen that as a result of coalescence of interfacial droplets, the number of datapoints decreased steadily over time, going from 63 on day 8 to 39 on day 12, and to 36 on day 16. Correspondingly, droplet−droplet coalescence led to an increase in the droplet size, as seen from the decrease in the number of datapoints with relatively large values of **a** and $\mathbf{A}_{vor}$. The size of the modified Voronoi cell, $\mathbf{A}_{vor}$, positively correlated with the size of the droplet, **a**, with relatively small dispersion. The linear relationship of **a** and $\mathbf{A}_{vor}$ strongly suggests that the growth of droplets is determined by a diffusion process.[32] Each interfacial droplet has an **a** and an $\mathbf{A}_{vor}$, and the ratio of $\mathbf{A}_{vor}$/**a** determines

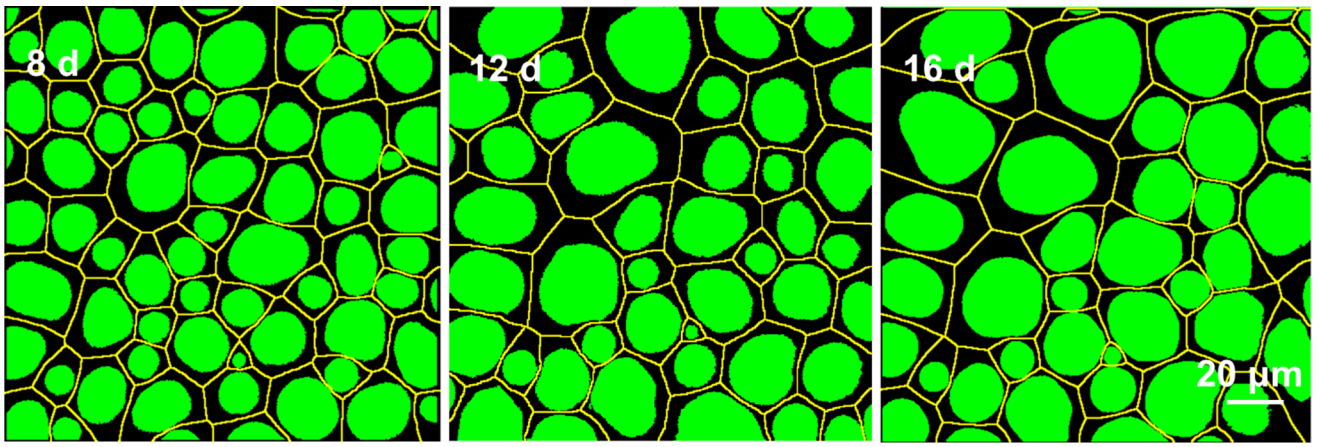

Figure 8. Modified Voronoi diagram of interfacial droplets on P-glass on days 8, 12, and 16. The interfacial droplet footprint has an area **a** and the modified Voronoi cell has an area $\mathbf{A}_{vor}$.

https://dx.doi.org/10.1021/acs.langmuir.9b03806
Langmuir 2020, 36, 5400−5407

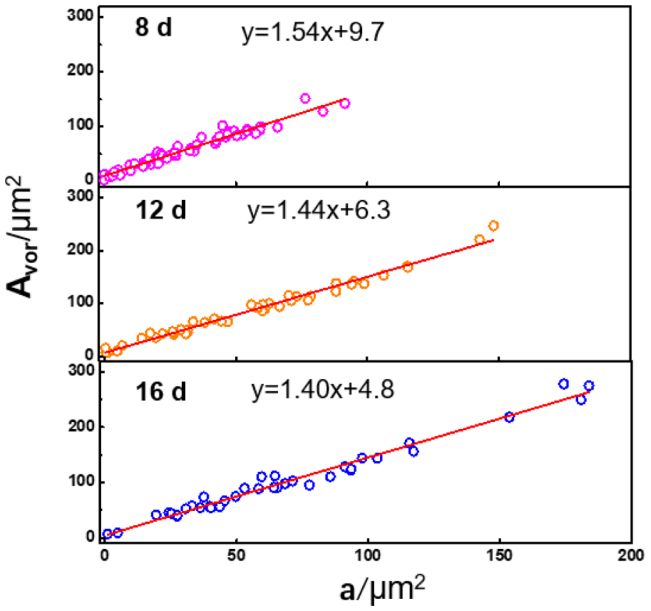

Figure 9. Projected area (**a**) vs modified Voronoi cell area ($\mathbf{A}_{vor}$) of interfacial droplets grown on P-glass on days 8, 12, and 16.

the slope. The slopes of the fitting curves were 1.54, 1.44, and 1.40 on days 8, 12, and 16, respectively. For different systems, the numbers of objects are different, and the values of **a** and $\mathbf{A}_{vor}$ vary from system to system. If there is a perfect statistical correlation between the Voronoi cell area and the droplet area, the slope of the scatter plots would be 1. The fact that the slope is initially larger than 1 but decreases in time suggests that the Voronoi cell area is an increasingly faithful representation of the droplet area as time progresses. Besides, the change in the slope also has a physical meaning. For example, the decrease of the slope is attributed to the coalescence of droplets, the slower decrease of the slope with the growth of the interfacial droplet means that the coalescence of droplets became less significant. Given that the interfacial droplets were dispersed at all times while growing in size, the size of each modified Voronoi cell would practically remain constant, but **a** would increase. Hence, we associate the increase in **a** for a given $\mathbf{A}_{vor}$ to the coalescence of interfacial droplets. It is noted that the slope decreased by 0.10 from day 8 to day 12, and further decreased only by about 0.04 from day 12 to day 16. The less decrement of the slope along incubation suggested that the coalescence of adjacent interfacial droplets happened at the early stage. However, we have not observed the occurrence of Ostwald ripening on interfacial droplet growth.[39] The main mechanism for droplet size evolution confirmed so far is that water in the bulk solution diffuses into the existing droplets and/or the droplets coalesce. Upon coalescence, there is no size preference that big droplets consume small droplets. It is noted that in our interfacial droplet system, the droplets are not free as those dispersed in the continuous phase, and the pinning on the surface restricts the droplets from moving and likely prevent Ostwald ripening. We are also aware that it is difficult to exclude the fact that nanodroplets exist in the system, and those invisible droplets with our current characterization technique may be consumed by big droplets and result in Ostwald ripening. A further investigation on the mechanism is needed.

Figure 10 shows the probability distribution function (pdf) of the normalized area $\mathbf{A}_{vor}/\langle\mathbf{A}_{vor}\rangle$ of modified Voronoi cells on P-glass for days 8, 12, and 16, where $\langle\mathbf{A}_{vor}\rangle$ represents the average area of $\mathbf{A}_{vor}$ together with the normalized γ-distribution,[40] given by

$$p(x) = \frac{343}{15}\sqrt{\frac{7}{2\pi}}\,x^{5/2}\,e^{-7x/2} \quad (1)$$

Motivated by the simple form of the distribution function in the one-dimensional (1D) case, a simple and compact analytical formula is proposed for approximating the Voronoi cell's size distribution function in the practically important 2D and 3D cases as well as by the authors. Equation 1 is the 2D case. The distribution of interfacial droplets is expected in the case of nucleation following a random Poisson process. This would be the case if interfacial droplets appear all at the same time. The comparison shows that the variance of **a** and $\mathbf{A}_{vor}$ is much larger than what is predicted by the γ-distribution. This larger variance can be traced back to the time evolution of the nucleation process. Some droplets nucleate first and compete with droplets that nucleate later in terms of growth. This interpretation can explain why after several days some droplets are much larger than others. The nucleation process of interfacial droplets that is random both in time and space has a larger standard deviation than that predicted by eq 1. This trend is also qualitatively consistent with our interpretation. When we compare the pdf of interfacial droplets on P-glass for different days, it shows that the distribution of the normalized droplet area has a significant variation from day 8 to day 12. This change is because of the disappearance of small droplets, which are large in number and therefore contribute significantly to the mean value (see e.g., the droplets in the top-left corner of the left-most panel of Figure 8). From day 12 to day 16, the probability distribution for P-glass reaches an approximate steady state: the droplets increase in size, but the

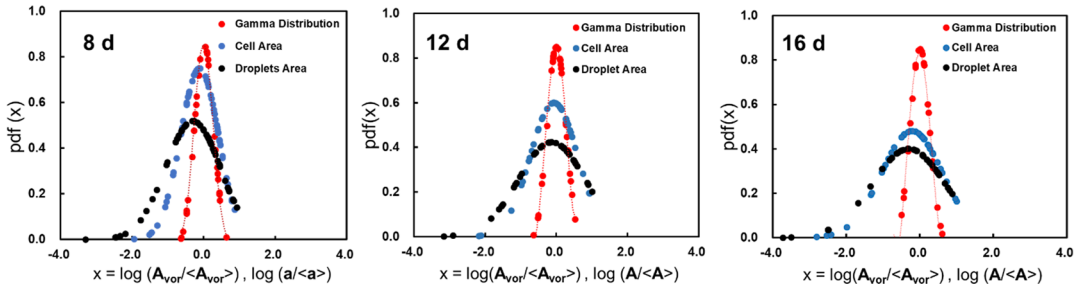

Figure 10. Normalized probability density function of the droplet area **a** and the modified Voronoi cell area $\mathbf{A}_{vor}$ of interfacial droplets grown on P-glass for days 8, 12, and 16. The red line shows the γ-distribution from eq 1, which would be expected for $\mathbf{A}_{vor}/\langle\mathbf{A}_{vor}\rangle$ in the case of a random spatial distribution of interfacial droplets.

https://dx.doi.org/10.1021/acs.langmuir.9b03806
Langmuir 2020, 36, 5400−5407

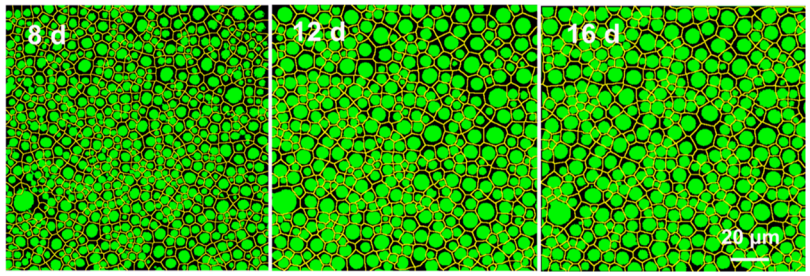

Figure 11. Modified Voronoi diagram of interfacial droplets on OTS-glass on days 8, 12, and 16. The interfacial droplet footprint has an area **a** and the modified Voronoi cell has an area $\mathbf{A}_{vor}$.

size ratio between large and small droplets remains practically constant. In order to see the evolution more clearly, we used a standard deviation of pdf to compare the change, see Table S1. The increment of the standard deviation of the pdf of the droplet area and the cell area on P-glass confirmed that the sizes of interfacial droplets become more polydispersed.

We now analyze modified Voronoi diagrams for interfacial droplets grown on OTS-glass. Figure 11 shows the modified Voronoi cells (depicted as yellow lines) of interfacial droplets grown on OTS-glass on days 8, 12, and 16. It can be clearly seen that from day 8 to day 12, the interfacial droplets grew, as confirmed from previous study that interfacial droplets absorbed water from the upper layer and/or merge together to become bigger droplets, and so did the modified Voronoi cells. However, from day 12 to day 16, the increase in the droplet and the modified Voronoi cell sizes were not obvious.

To characterize the changes more precisely, we therefore computed the areas and numbers of interfacial droplets and modified Voronoi cells using a MATLAB program. Figure 12

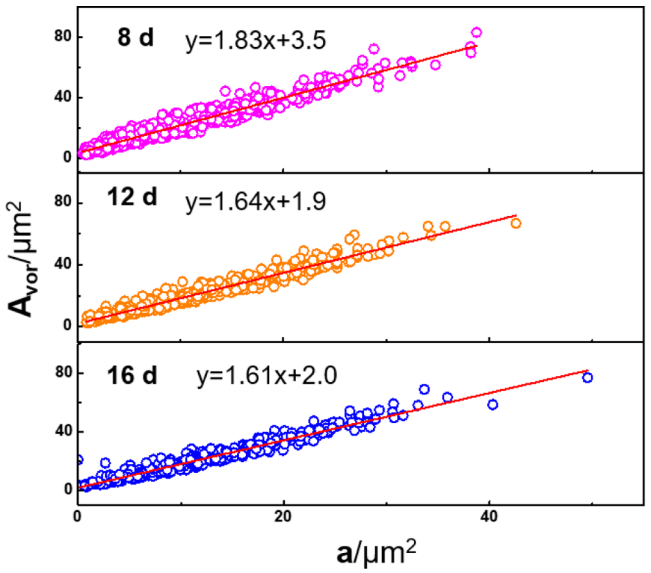

Figure 12. The projected area (**a**) versus modified Voronoi cell area ($\mathbf{A}_{vor}$) of interfacial droplets grown on OTS-glass on days 8, 12, and 16.

shows a scatter plot of **a** versus $\mathbf{A}_{vor}$ for interfacial droplets in a region of area 135 μm × 135 μm. The trends of changes in the droplet number and slope of **a** and $\mathbf{A}_{vor}$ for P-glass and OTS-glass were evidently very similar. The number of interfacial droplets on OTS-glass decreased with time, from 730 on day 8 to 464 on day 12, and 425 on day 16. The number of droplets decreased more sharply during the earlier stage of droplet evolution (from day 8 to day 12) than in the later stage (from day 12 to day 16) because as time went, the growth and the coalescence tend to slow down and finally stopped. Also, the data for OTS-glass fits a line quite accurately, proving again the dependence of **a** and $\mathbf{A}_{vor}$. The slope of the fitting line decreased from 1.83 on day 8 to 1.64 on day 12, and further to 1.61 on day 16, which confirmed that less coalescence would happen on the later stage compared with the early stage. It had the similar trend of slope change for interfacial droplets grown on P-glass.

Figure 13 shows the pdf of the normalized area $\mathbf{a}/\langle\mathbf{a}\rangle$ and $\mathbf{A}_{vor}/\langle\mathbf{A}_{vor}\rangle$ for OTS-glass on days 8, 12, and 16. Same as the interfacial droplets on P-glass, the experimental distribution of interfacial droplets on OTS-glass is much broader than the γ-distribution, which means that the interfacial droplets do not appear at the same time. However, different from P-glass, the distribution for OTS-glass instead shows that the number of droplets with a size comparable to the mean size grows in time, that is, the droplet size distribution becomes slightly less polydispersed as time progresses. This appears to be in contrast to the case of P-glass, where the polydispersity slightly increases with time. The standard deviation of the pdf of the droplet area on OTS-glass (seen in Table S1) becomes smaller, confirming that the sizes of interfacial droplets become more monodisperse. However, the change in the standard deviation of the cell area does not show a clear trend. While we do not have a simple explanation for this behavior, we notice that the distribution for OTS-glass at day 8 is significantly more symmetric than for P-glass, suggesting that the symmetry of the distribution at a given time may be one of the variables that determines the direction of change in the distribution at a later time. In summary, we used the modified Voronoi diagram to investigate the growth behavior and the spatial distribution of interfacial droplets on both hydrophilic and hydrophobic substrates. We found that interfacial droplets on both P-glass and OTS-glass had similar growth behavior in terms of the changes in both the droplet number and the slope of **a** and $\mathbf{A}_{vor}$. Interfacial droplets grow and merge together into larger droplets. The number of droplets decreases more sharply in the initial stages of the growth process. Besides, interfacial droplets on both P-glass and OTS-glass are not randomly distributed. The experimental distribution is much broader than the γ-distribution, suggesting that not all interfacial droplets appeared at the same time. However, a difference exists between P-glass and OTS-glass that the sizes of interfacial droplets become more polydispersed on P-glass, but more monodispersed on OTS-glass according to the time evolution of the pdf of the droplet area and the cell area on P-glass and OTS-glass.

https://dx.doi.org/10.1021/acs.langmuir.9b03806
Langmuir 2020, 36, 5400−5407

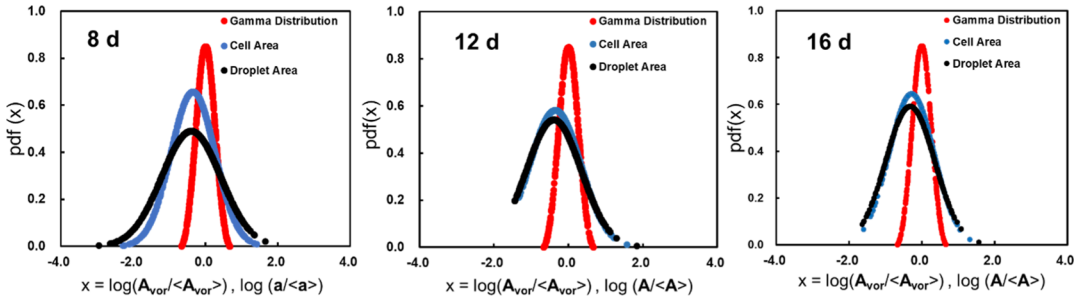

Figure 13. Normalized pdf of the droplet area **a** and the modified Voronoi cell area $\mathbf{A}_{vor}$ of interfacial droplets grown on OTS-glass for 8, 12, and 16 days. The red line shows the γ-distribution from eq 1, which would be expected for $\mathbf{A}_{vor}/\langle\mathbf{A}_{vor}\rangle$ in the case of a random spatial distribution of interfacial droplets.

CONCLUSIONS

For the first time, standard and modified Voronoi diagrams were used to investigate the spatial organization and growth behavior of interfacial droplets formed spontaneously at either hydrophilic (P-glass) or hydrophobic (OTS-glass) oil−solid interfaces, and a systematic comparison was made based on the effect of substrate wettability on the statistics of the droplet projected areas and Voronoi cell areas. In contrast to other groups' previous work in which mass diffusion occurs from the bulk liquid in contact with the substrate, nucleation is initiated by flowing an oversaturated solution;[41−43] in our case, the interfacial droplets formed spontaneously owing to the mass diffusion through a thin oil film from a water layer residing on top of the oil. The Voronoi analysis started from the projection of 3D confocal microscopy images at different times. The standard Voronoi diagram analysis was found to be unsuitable for the analysis of interfacial droplets on P-glass because the footprint of the droplets is not circular for this substrate. For this case, an analysis based on a modified Voronoi diagram was found to provide a better description of the statistics of interfacial droplets. In terms of OTS-glass, the standard Voronoi diagram was found to be unsuitable either for interfacial droplets. Although the shape of interfacial droplets is spherical, the standard Voronoi diagram constructed from the droplets' centers cannot distinguish interfacial droplets which grew in size but did not change in position. The use of a modified Voronoi diagram enabled to overcome this limitation. We observed that interfacial droplets grown on P-glass and OTS-glass had a qualitatively similar growth behavior. The interfacial droplets grow as a result of water diffusion through the thin oil film from the water layer, water absorbed through neighboring interfacial droplets, and droplet−droplet coalescence. The statistics of the modified Voronoi cells suggest that the droplet−droplet coalescence rate decreased with time in both the P-glass and OTS-glass substrate cases. The linear relationship of **a** and $\mathbf{A}_{vor}$ indicates that the formation of interfacial droplets is dominated by water diffusion. Analysis of the probability distribution of cell and droplet sizes suggests that the interfacial droplets are not distributed randomly and do not nucleate simultaneously. However, statistics shows the differences between OTS-glass and P-glass. By comparing the time evolution of pdf of interfacial droplets on both substrates, we found that the sizes of interfacial droplets become more polydispersed on P-glass, but more monodisperses on OTS-glass over time. Our investigation provides a framework for the analysis of the growth and spatial arrangement of interfacial droplets, enabling an improved understanding of the growth of droplets on hydrophilic and hydrophobic substrates.

ASSOCIATED CONTENT

Supporting Information

The Supporting Information is available free of charge at https://pubs.acs.org/doi/10.1021/acs.langmuir.9b03806.

Bright-field image of interfacial droplets formed on *n*-hexadecane and the OTS−glass interface when incubated in water for 2 min; and the standard deviation of pdf of droplet area and cell area on P-glass and OTS-glass (PDF)

Standard Voronoi diagram code and modified Voronoi diagram code (PDF)

AUTHOR INFORMATION

Corresponding Author

Zhongqiang Yang − *Key Laboratory of Organic Optoelectronics and Molecular Engineering of the Ministry of Education, Department of Chemistry, Tsinghua University, Beijing 100084, China*; orcid.org/0000-0002-9399-4424; Phone: +86-(0) 10-62796082; Email: zyang@tsinghua.edu.cn

Authors

Ran Zhang − *Key Laboratory of Organic Optoelectronics and Molecular Engineering of the Ministry of Education, Department of Chemistry, Tsinghua University, Beijing 100084, China*

Ran Andy Mei − *Key Laboratory of Organic Optoelectronics and Molecular Engineering of the Ministry of Education, Department of Chemistry, Tsinghua University, Beijing 100084, China*

Lorenzo Botto − *Process & Energy Department, Faculty of Mechanical, Maritime and Materials Engineering, TU Delft, Delft 2628 CB, The Netherlands*

Complete contact information is available at: https://pubs.acs.org/10.1021/acs.langmuir.9b03806

Author Contributions

The manuscript was written through contributions of all authors. All authors have given approval to the final version of the manuscript.

Notes

The authors declare no competing financial interest.

ACKNOWLEDGMENTS

This work was supported by the National Natural Science Foundation of China (21872078). L.B. acknowledges support from the European Research Council through the ERC StG project FLEXNANOFLOW (no. 715475).

REFERENCES

(1) Karpitschka, S.; Pandey, A.; Lubbers, L. A.; Weijs, J. H.; Botto, L.; Das, S.; Andreotti, B.; Snoeijer, J. H. Liquid Drops Attract or Repel by the Inverted Cheerios Effect. *Proc. Natl. Acad. Sci. U.S.A.* **2016**, *113*, 7403−7407.

(2) Méndez-Vilas, A.; Jódar-Reyes, A. B.; González-Martín, M. L. Ultrasmall Liquid Droplets on Solid Surfaces: Production, Imaging, and Relevance for Current Wetting Research. *Small* **2009**, *5*, 1366−1390.

(3) Bao, L.; Werbiuk, Z.; Lohse, D.; Zhang, X. Controlling the Growth Modes of Femtoliter Sessile Droplets Nucleating on Chemically Patterned Surfaces. *J. Phys. Chem. Lett.* **2016**, *7*, 1055−1059.

(4) Sun, Q.; Wang, D.; Li, Y.; Zhang, J.; Ye, S.; Cui, J.; Chen, L.; Wang, Z.; Butt, H.-J.; Vollmer, D.; Deng, X. Surface Charge Printing for Programmed Droplet Transport. *Nat. Mater.* **2019**, *18*, 936−941.

(5) Chu, Z.; Seeger, S. Superamphiphobic Surfaces. *Chem. Soc. Rev.* **2014**, *43*, 2784−2798.

(6) Ball, P. Nanobubbles are Not a Superficial Matter. *ChemPhysChem* **2012**, *13*, 2173−2177.

(7) Ni, X.; Choi, P. Wetting Behavior of Nanoscale Thin Films of Selected Organic Compounds and Water on Model Basal Surfaces of Kaolinite. *J. Phys. Chem. C* **2012**, *116*, 26275−26283.

(8) Pal, S. K.; Agarwal, A.; Abbott, N. L. Chemically Responsive Gels Prepared from Microspheres Dispersed in Liquid Crystals. *Small* **2009**, *5*, 2589−2596.

(9) Tawfick, S.; De Volder, M.; Copic, D.; Park, S. J.; Oliver, C. R.; Polsen, E. S.; Roberts, M. J.; Hart, A. J. Engineering of Micro- and Nanostructured Surfaces with Anisotropic Geometries and Properties. *Adv. Mater.* **2012**, *24*, 1628−1674.

(10) Jokinen, V.; Leinikka, M.; Franssila, S. Microstructured Surfaces for Directional Wetting. *Adv. Mater.* **2009**, *21*, 4835−4838.

(11) Boreyko, J. B.; Hansen, R. R.; Murphy, K. R.; Nath, S.; Retterer, S. T.; Collier, C. P. Controlling Condensation and Frost Growth with Chemical Micropatterns. *Sci. Rep.* **2016**, *6*, 19131.

(12) Kajiya, T.; Schellenberger, F.; Papadopoulos, P.; Vollmer, D.; Butt, H.-J. 3D Imaging of Water-Drop Condensation on Hydrophobic and Hydrophilic Lubricant-Impregnated Surfaces. *Sci. Rep.* **2016**, *6*, 23687.

(13) Xu, X.; Ma, L. Analysis of the Effects of Evaporative Cooling on the Evaporation of Liquid Droplets Using a Combined Field Approach. *Sci. Rep.* **2015**, *5*, 8614.

(14) Ellendt, N.; Ciftci, N.; Goodreau, C.; Uhlenwinkel, V.; Madler, L. Solidification of Single Droplets under Combined Cooling Conditions. *Mater. Sci. Eng.* **2016**, *117*, 012057.

(15) Seo, D.; Lee, J.; Lee, C.; Nam, Y. The Effects of Surface Wettability on the Fog and Dew Moisture Harvesting Performance on Tubular Surfaces. *Sci. Rep.* **2016**, *6*, 24276.

(16) Lalia, B. S.; Anand, S.; Varanasi, K. K.; Hashaikeh, R. Fog-Harvesting Potential of Lubricant-Impregnated Electrospun Nanomats. *Langmuir* **2013**, *29*, 13081−13088.

(17) Fessehaye, M.; Abdul-wahab, S. A.; Savage, M. J.; Kohler, T.; Gherezghiher, T.; Hurni, H. Fog-Water Collection for Community Use. *Renewable Sustainable Energy Rev.* **2014**, *29*, 52−62.

(18) Kim, H.; Yang, S.; Rao, S. R.; Narayanan, S.; Kapustin, E. A.; Furukawa, H.; Umans, A. S.; Yaghi, O. M.; Wang, E. N. Water Harvesting from Air with Metal-Organic Frameworks Powered by Natural Sunlight. *Science* **2017**, *356*, 430−434.

(19) Wang, F.-C.; Wu, H.-A. Pinning and Depinning Mechanism of the Contact Line During Evaporation of Nano-Droplets Sessile on Textured Surfaces. *Soft Matter* **2013**, *9*, 5703−5709.

(20) Wang, Y.; Zhao, J.; Zhang, D.; Jian, M.; Liu, H.; Zhang, X. Droplet Sliding: The Numerical Observation of Multiple Contact Angle Hysteresis. *Langmuir* **2019**, *35*, 9970−9978.

(21) Zhang, X.; Lu, Z.; Tan, H.; Bao, L.; He, Y.; Sun, C.; Lohse, D. Formation of Surface Nanodroplets under Controlled Flow Conditions. *Proc. Natl. Acad. Sci. U.S.A.* **2015**, *112*, 9253−9257.

(22) Bao, L.; Rezk, A. R.; Yeo, L. Y.; Zhang, X. Highly Ordered Arrays of Femtoliter Surface Droplets. *Small* **2015**, *11*, 4850−4855.

(23) Wang, Y.; Zaytsev, M. E.; Lajoinie, G.; The, H. L.; Eijkel, J. C. T.; van den Berg, A.; Versluis, M.; Weckhuysen, B. M.; Zhang, X.; Zandvliet, H. J. W.; Lohse, D. Giant and Explosive Plasmonic Bubbles by Delayed Nucleation. *Proc. Natl. Acad. Sci. U.S.A.* **2018**, *115*, 7676−7681.

(24) Zhang, L.; Zhang, Y.; Zhang, X.; Li, Z.; Shen, G.; Ye, M.; Fan, C.; Fang, H.; Hu, J. Electrochemically Controlled Formation and Growth of Hydrogen Nanobubbles. *Langmuir* **2006**, *22*, 8109−8113.

(25) Perumanath, S.; Borg, M. K.; Chubynsky, M. V.; Sprittles, J. E.; Reese, J. M. Droplet Coalescence is Initiated by Thermal Motion. *Phys. Rev. Lett.* **2019**, *122*, 104501.

(26) Zhang, R.; Liao, W.; Sun, Y.; Heng, J. Y. Y.; Yang, Z. Investigating the Role of Glass and Quartz Substrates on the Formation of Interfacial Droplets. *J. Phys. Chem. C* **2019**, *123*, 1151−1159.

(27) Zheng, Y.; Bai, H.; Huang, Z.; Tian, X.; Nie, F.-Q.; Zhao, Y.; Zhai, J.; Jiang, L. Directional Water Collection on Wetted Spider Silk. *Nature* **2010**, *463*, 640−643.

(28) Yang, Z.; Abbott, N. L. Spontaneous Formation of Water Droplets at Oil−Solid Interfaces. *Langmuir* **2010**, *26*, 13797−13804.

(29) Feng, S.; Wang, S.; Liu, C.; Zheng, Y.; Hou, Y. Controlled Droplet Transport on a Gradient Adhesion Surface. *Chem. Commun.* **2015**, *51*, 6010−6013.

(30) Zhang, R.; Wang, Y.; Yang, Z. Spatially Arranging Interfacial Droplets at the Oil-Solid Interface. *Soft Matter* **2020**, *16*, 107−113.

(31) Wang, Y.; Liu, G.; Hu, H.; Li, T. Y.; Johri, A. M.; Li, X.; Wang, J. Stable Encapsulated Air Nanobubbles in Water. *Angew. Chem., Int. Ed.* **2015**, *54*, 14291−14294.

(32) Lhuissier, H.; Lohse, D.; Zhang, X. Spatial Organization of Surface Nanobubbles and Its Implications in Their Formation Process. *Soft Matter* **2014**, *10*, 942−946.

(33) Xu, C.; Yu, H.; Peng, S.; Lu, Z.; Lei, L.; Lohse, D.; Zhang, X. Collective Interactions in the Nucleation and Growth of Surface Droplets. *Soft Matter* **2017**, *13*, 937−944.

(34) Li, Y.; Yang, Q.; Mei, R. A.; Cai, M.; Heng, J. Y. Y.; Yang, Z. Controlling the Accumulation of Water at Oil-Solid Interfaces with Gradient Coating. *J. Phys. Chem. B* **2017**, *121*, 6766−6772.

(35) Wang, Y.; Wang, Y.; Cai, M.; Li, H.; Yang, Z. Preparation and Growth of Interfacial Ultrasmall Water Droplets between Alkanes and Hydrophobic Solid. *Chem. J. Chinese Universities* **2018**, *39*, 2003−2009.

(36) Su, J. T.; Duncan, P. B.; Momaya, A.; Jutila, A.; Needham, D. The Effect of Hydrogen Bonding on the Diffusion of Water in n-Alkanes and n-Alcohols Measured with a Novel Single Microdroplet Method. *J. Chem. Phys.* **2010**, *132*, 044506.

(37) Schatzberg, P. Solubilities of Water in Several Normal Alkanes from C7to C16[1]. *J. Chem. Phys.* **1963**, *67*, 776−779.

(38) Zhao, H.; Beysens, D. From Droplet Growth to Film Growth on a Heterogeneous Surface: Condensation Associated with a Wettability Gradient. *Langmuir* **1995**, *11*, 627−634.

(39) Krichevsky, O.; Stavans, J. Correlated Ostwald Repening in Two Dimensions. *Phys. Rev. Lett.* **1993**, *70*, 1473−1476.

(40) Ferenc, J.-S.; Néda, Z. On the Size Distribution of Poisson Voronoi Cells. *Phys. A* **2007**, *385*, 518−526.

(41) Lohse, D.; Zhang, X. Surface Nanobubbles and Nanodroplets. *Rev. Mod. Phys.* **2015**, *87*, 981−1035.

(42) Parker, J. L.; Claesson, P. M.; Attard, P. Bubbles, Cavities, and the Long-Ranged Attraction between Hydrophobic Surfaces. *J. Phys. Chem.* **1994**, *98*, 8468−8480.

(43) Zhang, X. H.; Ducker, W. Interfacial Oil Droplets. *Langmuir* **2008**, *24*, 110−115.

https://dx.doi.org/10.1021/acs.langmuir.9b03806
Langmuir 2020, 36, 5400−5407